PAPER

Check for updates

Novel approach to monitor local tissue ischemia associated with pressure ulcers using an optical fibre carbon dioxide sensor†

Nadia Afroze,[ab] Serhiy Korposh, [iD] *[a] Ricardo Correia,[a] Peter R. Worsley,[c] Barrie R. Hayes-Gill,[a] Seung-Woo Lee[d] and Stephen P. Morgan[a]

In this paper, we describe the development of a novel approach to monitor local tissue ischemia associated with pressure ulcer using an optical fibre carbon dioxide sensor. Carbon dioxide (CO_2) is a potential biomarker for local tissue ischemia associated with pressure ulcer (PU) formation. Skin CO_2 measurement during loading could provide an earlier indicator for pressure induced tissue damage. This study presents a reflection mode optical fibre CO_2 sensor (OFCS) that was fabricated and evaluated for measuring skin CO_2 during mechanical loading. The optical fibre tip was coated with organically modified silica gel (ormosil) film (thickness 7.23 ± 0.52 μm) containing thymol blue using a dip coating process. Thymol blue has an absorption peak at a wavelength of ~600 nm with an amplitude proportional to CO_2 concentration. The OFCS had a typical response time of approximately 60 seconds and a recovery time of 400 seconds for a 0–5.5% CO_2 range. OFCSs were tested on the human skin of six healthy volunteers with corresponding CO_2 peak values ranging from 145 ppm to 429 ppm with a percent error range of 6–32.2%. The increase in CO_2 emitted from the skin during loading offers future promise for alerting the early stage of PU formation.

1. Introduction

Transcutaneous monitoring offers a non-invasive method of monitoring tissue gas tensions diffused through the skin.[1] For example, transcutaneous carbon dioxide pressure (T_CPCO_2) monitoring measures the level of CO_2 released from the skin that correlates with arterial partial pressure of carbon dioxide (P_aCO_2).[2] Partial pressure of carbon dioxide (PCO_2) indicates the CO_2 concentration dispersed in the blood and the interchange of this gas *via* the lungs.[3] Rising CO_2 may add more molecules to haemoglobin to remove the additional CO_2. Thus, a large rise of PCO_2 in the body's tissue is indicative of impaired blood flow and a transition to anaerobic metabolism.[4]

When the tissue is under mechanical loading in the form of pressure, or pressure in combination with shear, the systemic capillary network beneath the skin can be occluded. The corresponding gas exchange is reduced in the local tissues,

resulting in the accumulation of CO_2. In a recent systematic review, CO_2 was cited as the 'canary in the cage' for mechanically induced tissue damage.[4] CO_2 easily circulates into the extracellular area and localised tissue acidosis may arise. CO_2 may then disperse out of the cells and be found at the tissue's surface, resulting in an increase in measured T_CPCO_2. So, CO_2 measured from the skin was shown to have great potential as a biomarker for early pressure ulcer (PU) detection.[4] PU (or pressure injuries, bed sores, and decubitus ulcer) occurs when the skin is exposed to pressure, or pressure in combination with shear.[5] There is a relationship between tissue tolerance and the magnitude and duration of load,[6] which may also be affected by intrinsic factors such as comorbidities and tissue morphology.[7,8] PU appears over body areas with minimum body fat or muscle between the bone and skin, such as at the sacrum, spine, hips, shoulder blades, elbows, and heels.[9]

Commercial clinical devices exist to measure T_CPCO_2 in which a pH electrode detects the blood's pH changes that are proportional to the concentration of dissolved blood CO_2.[10] The main drawback of commercial T_CPCO_2 electrodes is they are bulky, preventing use for long periods on vulnerable body areas. In addition, for reliable measurement the electrode is typically heated to provide maximum vasodilation (37–42 °C), creating an adverse response to the local microvascular system. The commercial T_CPCO_2 electrode attaches to the skin *via* a contact gel, to ensure contact between the electrode and tissue.[11] This contact gel comprises a small quantity of sensitising elements,

[a] Optics and Photonics Research Group, Faculty of Engineering, University of Nottingham, Nottingham NG7 2RD, UK. E-mail: s.korposh@nottingham.ac.uk
[b] Electrical and Electronic Engineering, Faculty of Engineering, American International University-Bangladesh (AIUB), Dhaka, Bangladesh
[c] School of Health Sciences, University of Southampton, Southampton, UK
[d] Department of Chemical and Environmental Engineering, The University of Kitakyushu, Kitakyushu, Japan
† Electronic supplementary information (ESI) available. See DOI: https://doi.org/10.1039/d5sd00043b

which may cause an allergic reaction on sensitive skin.[12] As an example, a tc Sensor 92 probe (Radiometer, UK) is connected to a bulky TCM TOSCA monitor (approximately 4 kg), which is used to visualise and acquire data.[13]

Optical fibre sensing offers an alternative novel approach that has advantages over conventional probes for long-term monitoring of the skin. Optical fibre sensors (OFSs), such as the fabricated optical fibre CO_2 sensor (OFCS) presented in this paper, are small (in this paper, core diameter, Ø 62.5 μm and cladding diameter, Ø 125 μm), lightweight, passive, have low attenuation, are insusceptible to electromagnetic interference (EMI), and have high sensitivity and the capability to adhere to harsh environmental conditions.[14] For this application, the OFCS doesn't require a contact gel and temperature calibration compared to the commercial T_CPCO_2 electrode. In operation, the intensity of the OFS at a specific wavelength changes due to the level of CO_2 concentrations. Therefore, if comparable performance to electrochemical sensing could be achieved, then there is an opportunity for the OFCS to be used as a tissue health monitoring device.

In this paper, to the best of our knowledge, the first-in-kind measurement of CO_2 gas in the headspace emitted from skin is presented using both commercial CO_2 and novel OFCSs. A reflection mode OFCS is fabricated and tested with the ultimate objective of early prediction of PU formation. The optical fibre tip is coated with a colorimetric pH indicator dye, thymol blue, using a sol–gel coating process. Light from a halogen light source illuminates the optical fibre tip, and the reflected light (proportional to CO_2) is detected. Although the OFS CO_2 sensors have been developed previously for breath and environmental CO_2 detection, skin gas is measured for the first time.[15] Thus, it represents a novel application of an OFS to intact skin CO_2 measurement during loading and opens new possibilities for real-time, reliable early prediction and diagnosis of PU formation.
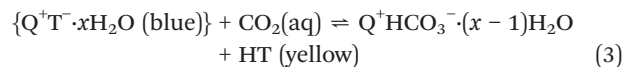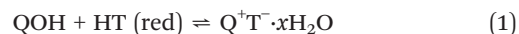
2. Materials & methods

2.1 Materials

Tetraethyl orthosilicate or tetraethoxysilane (TEOS), triethoxymethylsilane (MTEOS), ethanol, thymol blue (TB), tetramethylammonium hydroxide (TMAH) (10 wt% in H_2O), and Triton X-100 were all obtained from Sigma-Aldrich, UK. Isopropyl alcohol (IPA) and 2-propanol (≥99.5%) were obtained from Fisher Chemical, UK. CO_2 (5% argon (Ar) mixture) was obtained from Ryvalgas, UK and nitrogen (N_2) (oxygen (O_2) free) was obtained from BOC, UK. An OM1 Multimode (MM) silica core, silica cladding (core diameter, Ø 62.5 μm and cladding diameter, Ø 125 μm) optical fibre and Pigtail Easystrip (ST, Length 1.5 m) were purchased from all4fiber GmbH, Austria.

2.2 Sensing mechanism for CO_2

Two detectable ranges are available for TB as a pH indicator dye. Its colour changes from red to yellow at pH levels of 1.2 to 2.8 and from yellow to blue at pH levels of 8.0 to 9.2. The gas exchange between the film and the environment is controlled by the prepared sol–gel film doped with TB and TMAH. The colour change that occurs during the CO_2 reaction can be explained as follows:[15]

$$QOH + HT \text{ (red)} \rightleftharpoons Q^+T^- \cdot xH_2O \tag{1}$$

$$CO_2(g) \rightleftharpoons CO_2(aq) \tag{2}$$

$$\{Q^+T^- \cdot xH_2O \text{ (blue)}\} + CO_2(aq) \rightleftharpoons Q^+HCO_3^- \cdot (x-1)H_2O + HT \text{ (yellow)} \tag{3}$$

where QOH is TMAH, HT is the acidic version of TB, T^- is the deprotonated TB ion and Q^+ is a tetramethylammonium ion. $Q^+T^- \cdot xH_2O$ is the ion pair formed within the sol–gel film by acidic TB and TMAH, which causes the colour shift from red to blue when the protonation state of TB changes [eqn (1)]. Gaseous CO_2 transforms into aqueous CO_2 once it infuses from the exterior into the sol–gel film. The hydrated water molecule combines with CO_2 to produce a hydrogen ion, which transforms from T^- to HT, as shown in eqn (3), and the colour changes from blue to yellow.[16]

2.3 Sensor fabrication

A stirrer (Stuart Hotplate Stirrer, US152, Cole-Parmer, UK) was used to mix the chemicals on each occasion. The mixture was prepared at room temperature (approximately 20 °C), and the heat-controlled knob of the plate was turned off during this mixing process. The speed was chosen at an arbitrary value of 220 rpm while mixing the chemicals. 1.8 mL MTEOS was stirred with 200 μL TEOS for 10 min in a 20 mL glass vial to prepare an organically modified silica (ormosil) solution. Next, 6 mL ethanol was added to the solution and stirred for another 10 min. TB powder (22 mg) was added to the solution and stirred for another 15 min. Another mixture of Triton X-100 (0.1 mL) and deionized water (DI H_2O) (0.9 mL) was added to the solution and stirred for another 15 min. Finally, 500 μL of TMAH was added to the solution, and the glass vial was covered and stirred for 1 hour using the above-mentioned automatic stirrer before dip-coating.[15]

The jacket and buffer coating of the optical fibre were removed using a fibre optic stripper (JIC 375, Jonards Tools, USA). The optical fibre cladding was cleaned using IPA and clean wipes (Stickler Benchtop, MCC-WFW, Thorlabs, UK). The optical fibre tip was cleaved at an angle of 90° using a fibre-optic precision cleaver (VF-15H, Inno Instrument, Germany) and then dip-coated 4 times employing a commercial dip-coating unit (HO-TH-02, Holmarc Opto-Mechatronics Pvt. Ltd., India) with a withdrawal speed of 3 mm s^{-1}, as shown in Fig. 1. The drying interval was 2 min between each coating layer under ambient conditions. Before use, the coated fibres were placed inside a pure N_2 (CO_2 and humidity-free) environment for 24 hours.[15] Sensors were characterised through scanning electron microscopy (SEM), and the reflectance spectrum of the sensor at each deposited layer was measured, as shown in Fig. 1.
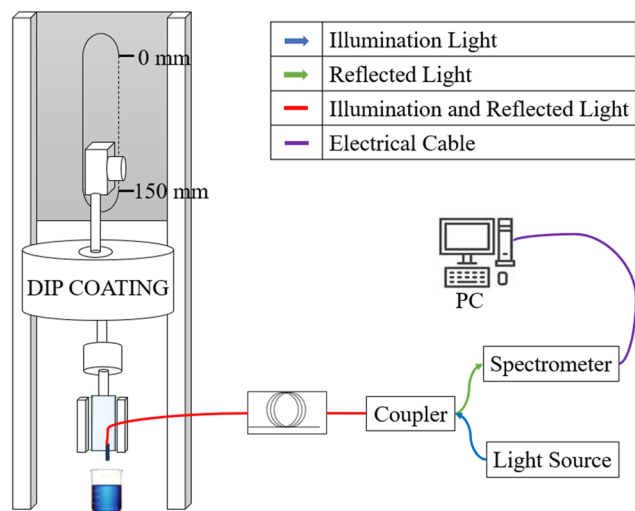
Fig. 1 Experimental set-up for the coating process onto an optical fibre tip.

The non-ionic surfactant Triton X-100 was used in the solution for sensor fabrication. Triton X-100 provides smooth surface texture and prevents cracking by raising the molecular mass and lowering the interfacial energy and capillary stresses when it was added to the pore liquid.[16–18]

2.4 Sensor calibration

The reflection spectrum of the OFCS was measured using an experimental design shown in Fig. 2. A halogen light source (HL-2000, Ocean Insight, UK) was connected to a fixed MM fibre optic attenuator (FA14M, 1.40 mm gap length, Thorlabs, UK) through an SMA fibre optic patch cable (M92L01, core diameter, Ø 200 μm and cladding diameter, Ø 220 μm, Thorlabs, UK) to reduce the optical power and photobleaching of the TB coating.

The OFCS tip was illuminated by a halogen light source through a 1 × 2 MM Coupler 50/50 (500-60336-61-3, core diameter, Ø 62.5 μm, cladding diameter, Ø 125 μm, and ideal loss/port 3 dB, Lightel, USA), and the reflected light was captured using an optical spectrometer (FLAME-S-VIS-NIR-ES, optical resolution ∼0.1 nm, Ocean Insight, UK), linked to a computer for data analysis.

A commercial CO_2 datalogger (K33 ICB 10% CO_2 sensor, **https://CO2Meter.com**, USA) independently measures the CO_2 concentrations in a gas chamber over the range of 0–100 000 ppm. The OFCS and commercial CO_2 datalogger are housed inside a custom-made gas chamber (270 mm (L) × 195 mm (W) × 105 mm (H), BPA-free plastic airtight container, Nisbets Plc, UK) with routes for gas inflow and outflow.

A mixture of N_2 and CO_2 controlled the CO_2 concentration inside the chamber. The reflection intensity of the OFCS and CO_2 concentration (from the commercial CO_2 datalogger) were recorded using SpectraSuite Software and Gaslab Software respectively. Pure N_2 gas was flushed inside the gas chamber until the CO_2 was removed (0 ppm) before the experiment commenced. A polytetrafluoroethylene (PTFE) flow meter (WZ-03216-52, Cole-Parmer, UK) was used to control the step-by-step variation of CO_2 concentration inside the gas chamber via the gas-in route. At least 10 min was required for the CO_2 concentration inside the gas chamber to stabilise. The minimum data recording interval possible was 20 seconds for the commercial CO_2 datalogger. The integration time (data recording interval) was set to 1 s for the spectrometer for signal averaging purposes.

Additional calibration was also carried out in a lower CO_2 range (0–1200 ppm) using a more sensitive commercial sensor (CozIR-A 10 000 ppm CO_2 sensor, CM-0120, **https://CO2Meter.com**, USA). In this case, both the OFCS and CO_2 sensor were placed inside the holding unit used in the skin studies described in section 2.5.

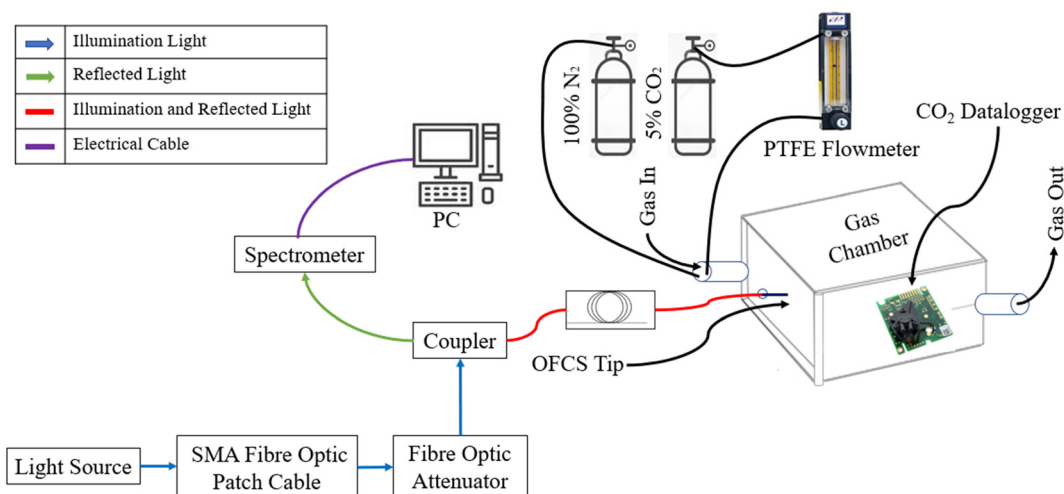To normalise sensor response, raw spectra values were converted to absorbance, A, using the formula:[15]

Fig. 2 Experimental set-up for CO_2 calibration of the OFCS.

$$A = 2 - \log_{10}\left[\left(\frac{I_r}{I_0}\right) \times 100\right] \qquad (4)$$

where I_0 is the light intensity reflected from the optical fibre tip without any sensing film and I_r is the light intensity after an interaction with the coated film.[15] Calibration was initially performed over a very wide range of CO_2 concentrations (0–50 000 ppm) to demonstrate the response of a single sensor. A narrower range (250–1150 ppm) more representative of skin CO_2 values was then measured for all sensors with smaller (60 ppm) CO_2 concentration step size.

2.5 Skin CO_2 measurement

For placing both the OFCS and CO_2 sensor at the same position on the skin, a polylactic acid (PLA) (MP002267, Multicomp Pro, Farnell, UK) holder (diameter = 43 mm) was 3D-printed. The set-up for skin CO_2 measurement is shown in Fig. 3. The holder also contained a PTFE film (FLONFILM™ 100, Polyflon, UK) as it prevented humidity from reaching the OFCS tip but didn't affect CO_2 diffusion. The holder is then placed on a volunteer's forearm before loading.

The holder was fabricated in the same shape as a commercial CO_2 sensor (CozIR-A 10 000 ppm CO_2 sensor, CM-0120, **https://CO2Meter.com**, USA) with an external body diameter of 43 mm and a sensor head aperture of 18 mm.[19] The optical fibre sensor placed within the holder measures the integrated concentration of CO_2 emitted from the skin in the local environment covered by the holder. This allows direct comparison of the OFCS and commercial CO_2 sensor. There is a trade-off between the size of the holder (sensor aperture diameter and collection volume) and the CO_2 concentration.

A loading machine was designed and implemented which consists of a weight holder, a steel rod with a ball bearing, and a PLA circular plate. The circular plate presses on the holder containing the CO_2 sensors. The weight of the empty holder with the steel rod was ~0.5 kg and additional slotted masses (100 g) were placed inside the weight holder to increase the load. The contact area between the skin and the holder is 1198 mm². The loading machine provided pressures in the range between 4 kPa and 17 kPa for the skin CO_2 measurement, equivalent to 0.5 kg and 2.1 kg loads, respectively. The loading protocol for each volunteer is firstly 5 min at 0.5 kg, next 10 min at 2.1 kg, and lastly 5 min at 0.5 kg.

To ensure that sufficient levels of CO_2 were emitted from the skin during loading, a heated disc (3D hot & cold therapy disc, Neo G, UK) was placed on the skin alongside a thermocouple probe to monitor the temperature. A heated disc needs to be warmed at 42–45 °C to increase local skin blood flow due to the vasodilation of the capillary loops.[19] A bandage and foil blanket (QZ9200, JaxFirstAid, UK) were wrapped around the disc to prevent heat loss. Tests were conducted on 6 healthy volunteers (4 men and 2 women, average age 28.5 ± 5.6 years old, average height 169.4 ± 11.2 cm, and average weight 68.5 ± 10.1 kg) under ethical approval obtained from the Faculty of Engineering Ethics Committee, University of Nottingham (UoN).

Although this study only included healthy participants, the skin measurement method replicates previously conducted research at different institutions.[21,22] Our future work will focus on testing patients that are susceptible to pressure-induced tissue damage. This is the first time that CO_2 in the gas phase has been detected from the skin under different loadings using an OFCS.
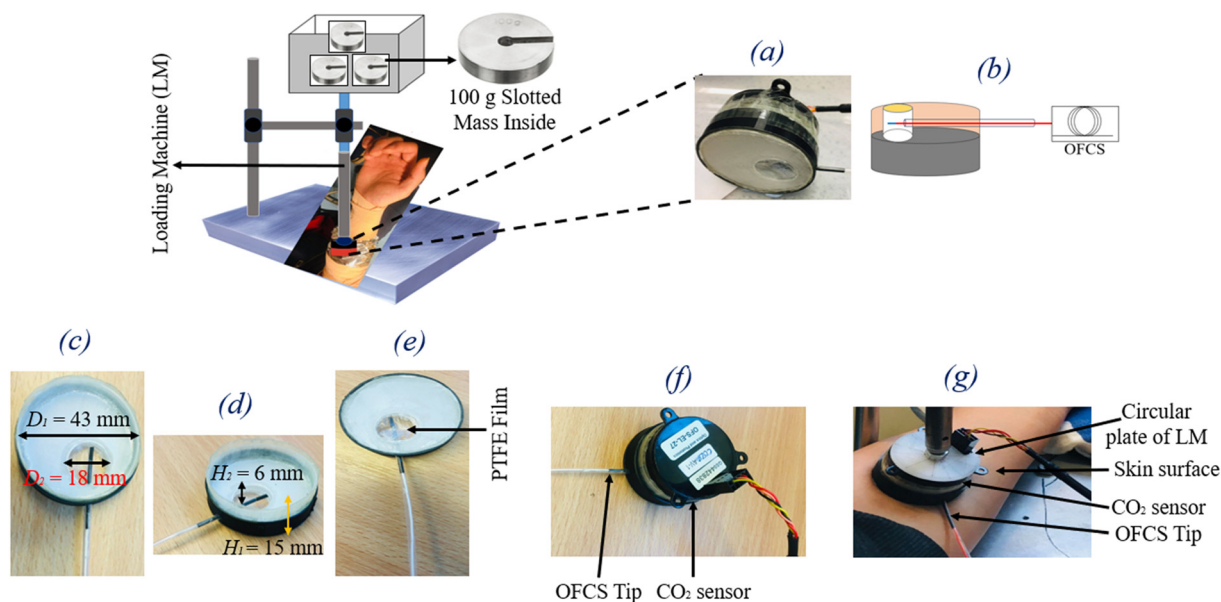
Fig. 3 Experimental set-up for monitoring CO_2 emitted from wrapped human skin during loading using the OFCS and commercial CO_2 sensor: (a) magnified image, (b) schematic diagram, (c) top view, (d) side view, and (e) bottom view of the PLA holder and top view of this holder on (f) a wooden surface without a loading arm and (g) a skin surface with a loading arm.
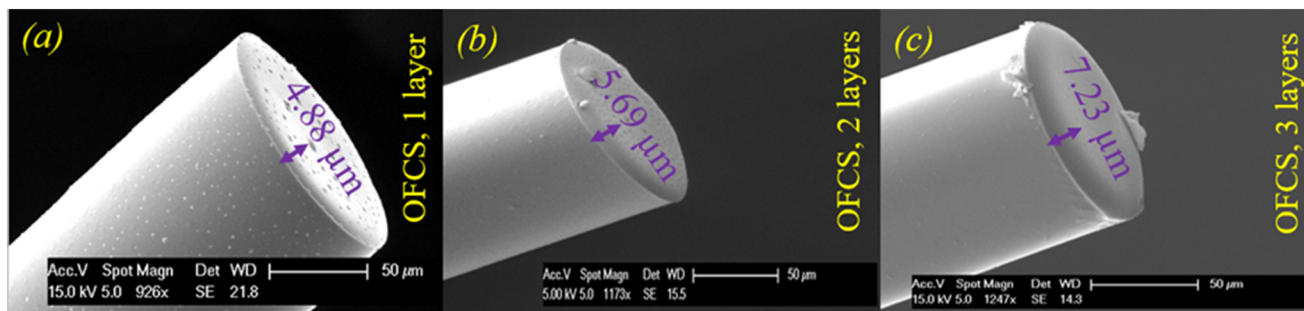
Fig. 4 SEM images of the OFCS tip with (a) 1 layer, (b) 2 layers and (c) 3 layers. Scale bar = 50 μm.

Previous research using $T_C PCO_2$ measurements provide a framework for future studies using an OFCS. In particular, the outcome of various loading regimes, comprising repetitive and prolonged loading, on the normal $T_C PCO_2$ value at locations adjacent to bony prominences in 14 healthy participants was monitored using a transcutaneous electrochemical sensor.[21] In other research, 80 inpatients in Beijing Chaoyang Hospital were measured at the anterior chest in a lateral position and sacrococcygeal regions in lateral and supine positions using a TCM CombiM device (Radiometer A/S, Denmark).[22] Among these 80 inpatients, 31 (25 male, 6 female, aged 41–88 years old and average age of 71.56 ± 12.30 years) of the cases were in the high-risk group and 49 cases (32 male and 17 female, aged 40–87 years old and average age of 66.94 ± 15.23 years) in the low-risk group. The study concluded that the values of $T_C PO_2$ and $T_C PCO_2$ are sensitive to the change of pressure imposed on the measured region and to the risk status of a pressure injury when a pressure is imposed. Moreover, the magnitude of change in $T_C PO_2$ and $T_C PCO_2$ is higher in patients with a high risk of a pressure injury compared with those who have a low risk.[22]

The reflection spectrum of the OFCS was recorded with an integration time of 1 second using SpectraSuite Software. CO_2 concentrations from the commercial sensor were recorded every 20 seconds using Gaslab Software. This experiment took approximately 20 min for each participant.

2.6 Live subject statement

All experiments on human volunteers were performed in accordance with the principles and standards of the Declaration of Helsinki: Ethical Principles for Medical Research Involving Human Subjects, and approved by the ethics committee at the Faculty of Engineering Ethics Committee, University of Nottingham (UoN). Informed consents were obtained from human participants of this study.

3. Results

3.1 Sensor characterisation

Fig. 4(a)–(c) show three SEM images of the OFCS tip with 1, 2, and 3 layers (including the film thickness), respectively. The film thickness of 4.88 ± 0.54, 5.69 ± 0.75, and 7.23 ± 0.52
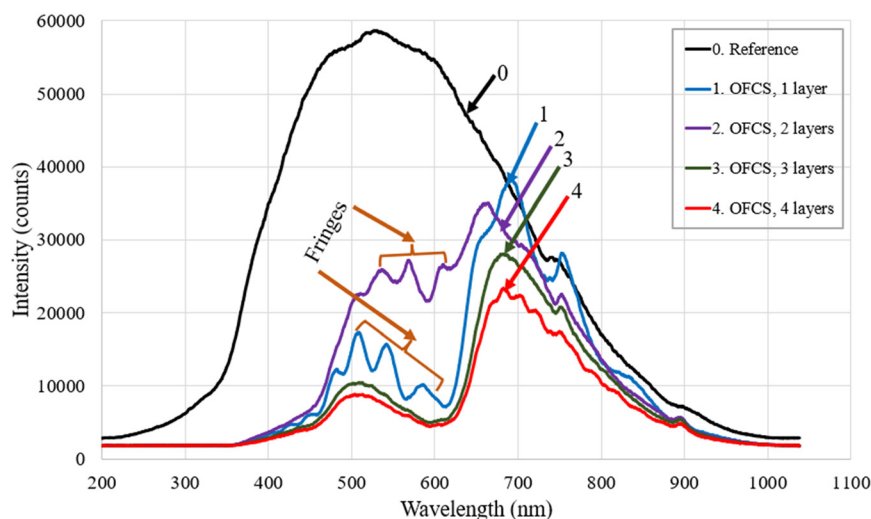

Fig. 5 Reflection spectra of the OFCS after coating and each curve represents an additional coated layer; black line 0, unmodified optical fibre tip; blue line 1, modified with 1 layer; purple line 2, modified with 2 layers; green line 3, modified with 3 layers; red line 4, modified with 4 layers.

μm was achieved for the OFCS with 1, 2, and 3 layers, respectively.

Fig. 5 demonstrates a typical reflection spectrum after each coating cycle on the optical fibre tip during the coating process. Interference fringes for 1 layer and 2 layers of coating that can be seen as the coated layer on the optical fibre tip create a Fabry–Perot interferometer (FPI) cavity. FPI fringes are visible due to the differential phase of reflected light between the optical fibre interface to the coated thin film and the interface of the coated thin film to ambient air. The absorption window was selected from 500 nm to 700 nm according to TB's absorption characteristics.[20] The fringes become less visible for 3 layers and 4 layers of coating, as shown in Fig. 5, as the thicker sol–gel coating makes a large optical path difference between the fibre and the film. A continuous distribution of interference fringes with a range of phase differences that average to zero results in decreasing fringe visibility.[21] Due to the increased absorption value induced by the thick film based on eqn (4), the reflected intensity at a wavelength of approximately 600 nm diminishes as each layer is deposited.[15]

In Fig. 5, the intensity of the bare fibre (unmodified optical fibre tip) is 54 500 counts at a wavelength of 600 nm. The intensities of the optical fibre tip with 1, 2, 3, and 4 layers are 23 900, 8300, 5200, and 4600 counts at a wavelength of 600 nm, respectively. The intensity decreases due to the number of layers or coating thickness increment according to the Lambert–Beer Law (which describes how the intensity of a light beam exponentially decreases as it travels through a purely absorbing medium[25]).

Fig. 6(a) and (b) illustrate the reflection spectrum of the bare fibre, and the reflection and absorption spectra of the OFCS for maximum (45 000 ppm or 4.5% CO_2) and minimum (0 ppm or 0% CO_2) CO_2 concentrations, respectively. The highest absorption peak due to the changes in CO_2 concentration is achieved at a wavelength of approximately 600 nm, as shown in Fig. 6(b). A noticeable change in reflection intensity and absorbance at a wavelength of approximately 600 nm is observed, and this is used for CO_2 measurement.

3.2 Calibration (results for high CO_2 concentration, ~0–50 000 ppm)

Fig. 7 shows the step-up and down of the response (reflection intensity) of an OFCS at a wavelength of approximately 600 nm using the experimental design detailed in Fig. 2. The reflection intensity of the OFCS increases with rising CO_2 concentration from 0 ppm (0% CO_2) to around 46 000 ppm (4.6% CO_2) and the reflection intensity of the OFCS decreases with falling CO_2 concentration from around 46 000 ppm (4.6% CO_2) to 0 ppm (0% CO_2). Fig. 7b shows how the average reflection intensity of the OFCS is related to the average value of CO_2 concentration *via* a polynomial fitting curve.

Fig. 8 illustrates the calculation of the response and recovery times of the OFCS at a wavelength of around 600 nm using the set-up shown in Fig. 2. The response time was calculated when the OFCS was inserted into the gas chamber with around 55 000 ppm (5.5% CO_2) from ambient air (around 400 ppm). The recovery time was measured when the OFCS was taken out from the gas chamber of almost 55 000 ppm (5.5% CO_2) to ambient air (nearly 400 ppm). The response time of the OFCS is 60 seconds, which is the time required to rise from 10% to 90% of the final value of reflection intensity. However, the recovery time of the OFCS is 400 seconds which is required to drop from 90% to 10% of the final value of reflection intensity.

3.3 Calibration (results for low CO_2 concentration, ~250–1150 ppm)

Fig. 9 shows an example of an OFCS (OFCS 1) response using the set-up shown in Fig. 2. Responses for other sensors are shown in Fig. A.1–A.5 [ESI†].
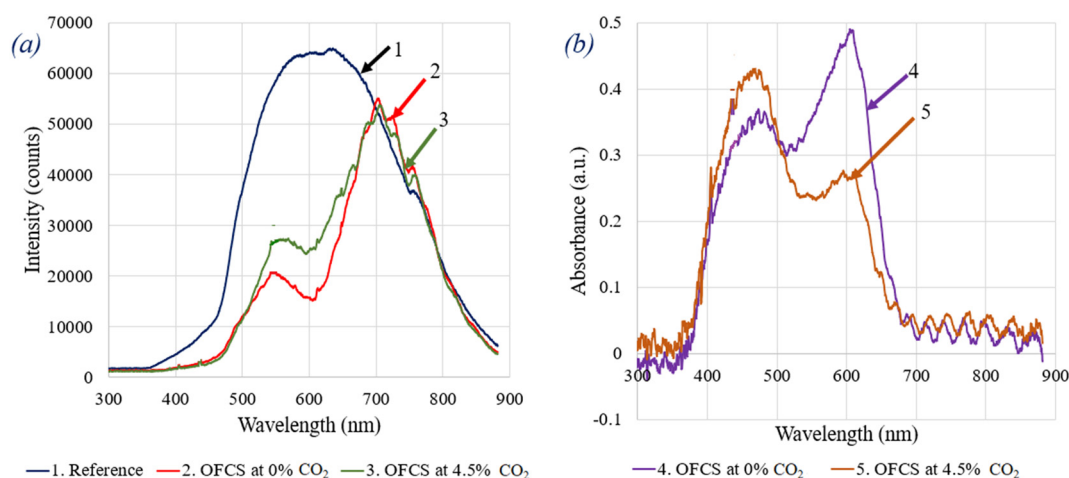
Fig. 6 (a) Reflection spectra of the OFCS; black line 1, reference signal from the reflection spectrum of the bare fibre; red line 2, intensity of the OFCS at minimum concentration; green line 3, intensity of the OFCS at maximum concentration. (b) Absorption spectra of the OFCS; purple line 4, absorbance of the OFCS at minimum concentration; orange line 5, absorbance of the OFCS at maximum concentration.
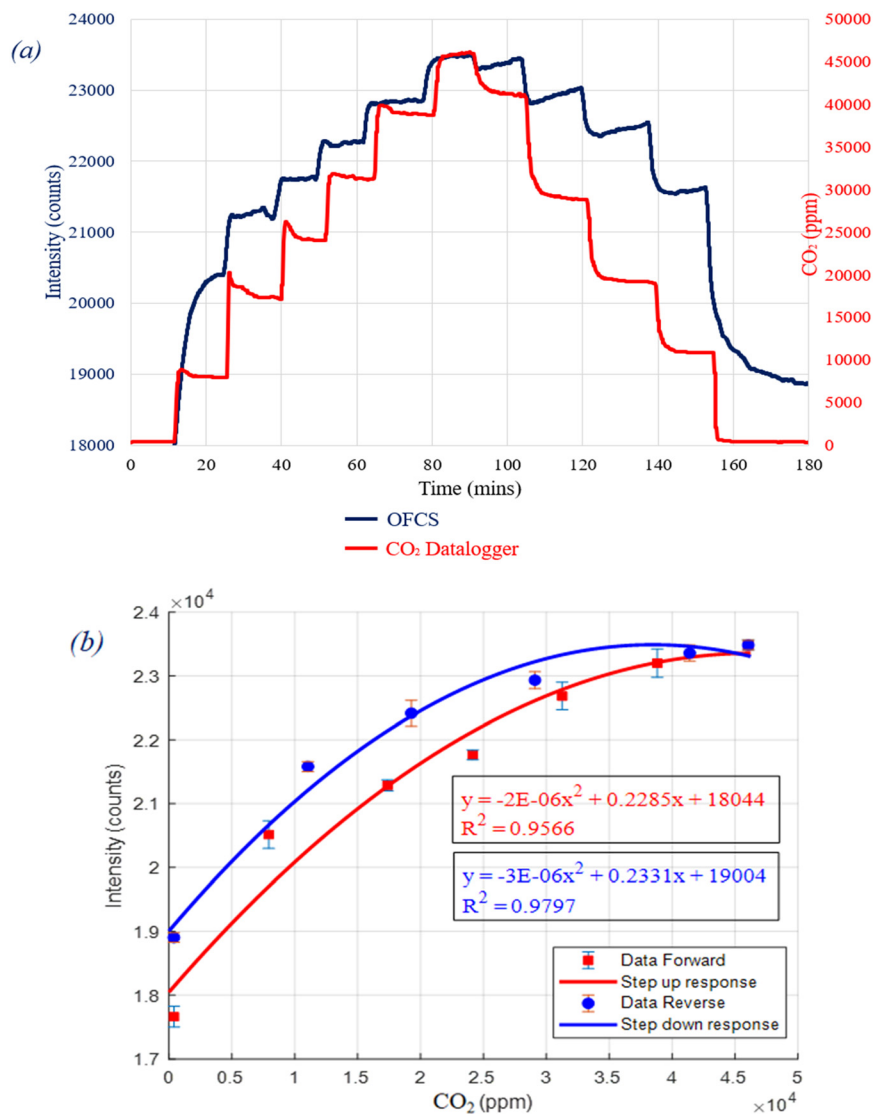
Sensors & Diagnostics

Paper

Fig. 7 Step-up and down response of the OFCS at a wavelength of 600 nm for different CO_2 concentrations; a) response with time; b) polynomial fitting of reflection intensities of the OFCS responses with increasing and decreasing CO_2 concentrations.

The intensity (counts) was plotted with respect to the CO_2 (ppm) in Fig. 9. The reflection intensity of each OFCS at a wavelength of 600 nm linearly increased with rising CO_2 concentration, measured at 60 ppm intervals. This linear equation represents the sensitivity of OFCS 1 as 0.9739 counts per ppm. The sensitivity was used to calculate the variation in the OFCS's response (intensity) and the commercial CO_2 sensor during the skin CO_2 measurement.

Fig. A.1–A.5 [ESI†] illustrate the linear relationship between the intensity (counts) and CO_2 (ppm) for OFCSs 2–6. Subtracting the offset of the linear fit allows the responses to be compared on the same graph. Fig. 10 shows that although all the responses are linear there is variability, likely due to non-uniform coating across the sensors. However, these lines can be used individually for calibration in the skin loading experiment.

3.4 Skin CO_2 measurement during loading

Fig. 11(a) shows the changes in reflection intensity at a wavelength of 600 nm and the CO_2 concentration (from the commercial CO_2 sensor) during loading on volunteer 1's forearm using the set-up shown in Fig. 3. The reflection intensity and CO_2 concentration are relatively stable for the first 12 min when OFCS 1 is under ambient conditions. The reflection intensity and CO_2 concentration increase when OFCS 1 and the warmed therapy disc are placed on the forearm with the load (0.5 kg) for 5 min. Again, the reflection intensity and CO_2 concentration increase when the load (2.1 kg and 0.5 kg) is applied for the next 10 and 5 min, respectively. Finally, the reflection intensity and CO_2 concentration decrease when OFCS 1 is moved from the skin to air for 18 min. It should be noted that the signal does not return to baseline, and this is discussed in more detail in section 4.
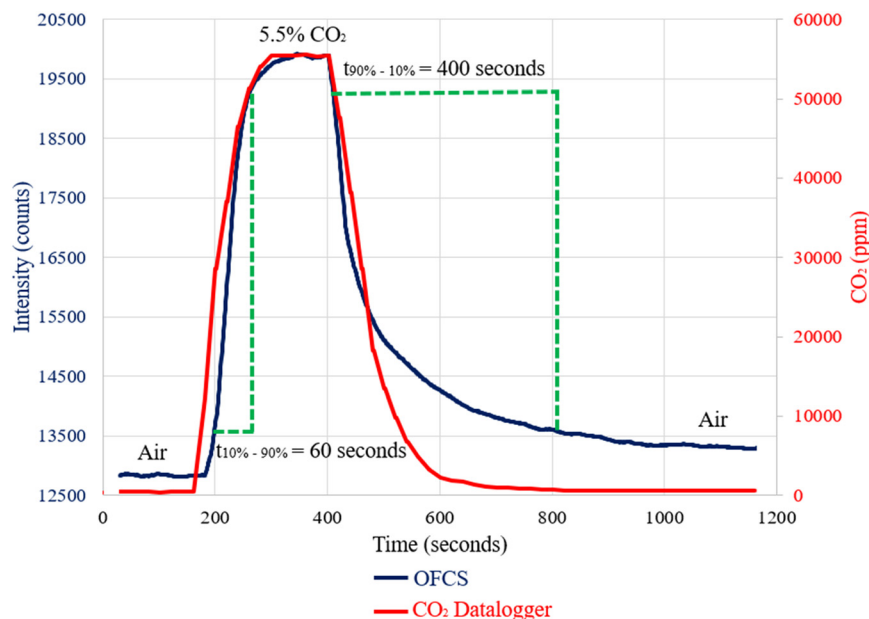
Fig. 8 Response and recovery time measurement of the OFCS for 5.5% CO_2 at a wavelength of 600 nm.
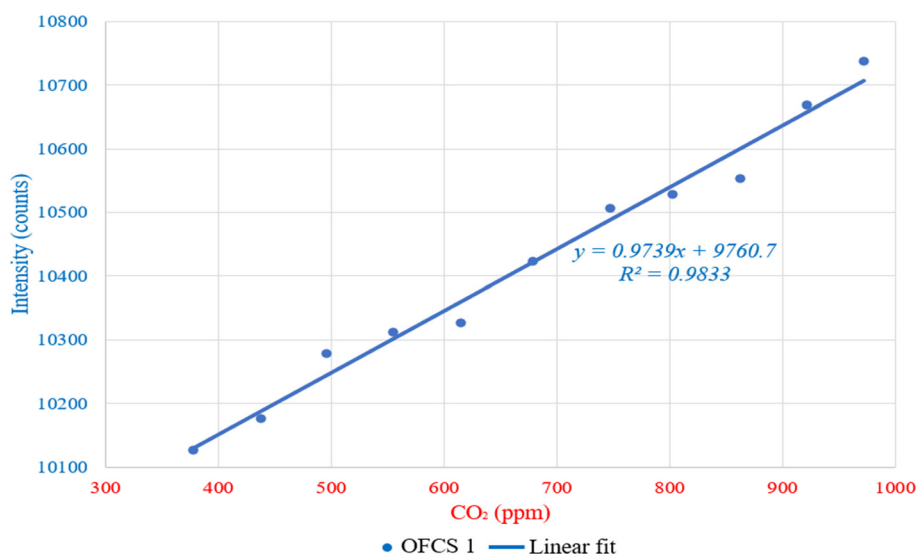

Fig. 9 Linear fitting of reflection intensities of OFCS 1 to different CO_2 concentrations at a wavelength of 600 nm.

Volunteer 1's skin temperature is also illustrated in Fig. 11(b). The temperature decreases gradually due to the cooling of the therapy disc. It should be noted that the skin temperature after the therapy disc is cooled is below normal body temperature (37 °C) as it is outside and interacts with the external environment. Fig. A.6(b)–A.10(b) [ESI†] present the skin temperature of volunteers 2–6, respectively and follow the same trend as Fig. 11(b).

To maximise CO_2 emission, skin temperature would ideally remain at an elevated level throughout the experiment. However, a limitation of this study is that the temperature decreases gradually due to the cooling of the therapy disc. Fig. A.6(b), (d) and (f)–A.10(b), (d) and (f) [ESI†] present the skin

temperature of volunteers 2–6, respectively, and follow the same trend as Fig. 11(b). T_CPCO_2 probes utilise a temperature correction factor[13] and in the future, a similar approach could be applied to OFCS probes.

The reflection intensity of OFCSs 2–6 during the skin CO_2 measurement is shown in Fig. A.6a–A.10a [ESI†], respectively. All follow the same trends as Fig. 11 but with errors when compared to the commercial sensor which are summarised in Table 1. The errors obtained are the CO_2 change between the baseline and peak loading of the skin for the OFCS and commercial CO_2 sensor.

The purpose of the 3 trials is to observe the variation in the response of the OFCSs (OFCS 1–6) and commercial CO_2 sensor
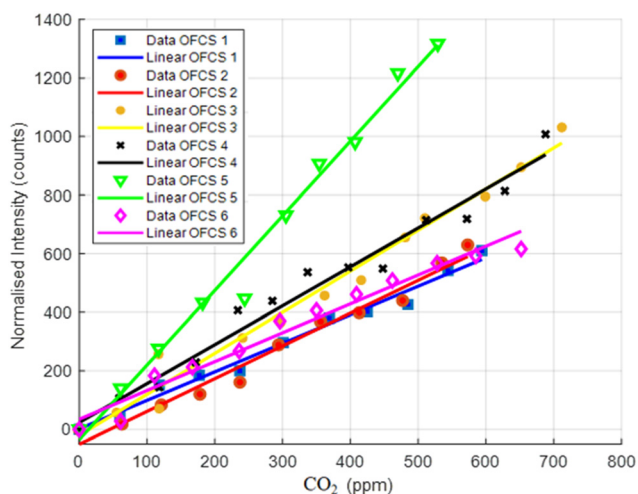
Fig. 10 Linear fitting of normalised intensities of 6 OFCSs (OFCS 1–6) to different CO_2 concentrations at a wavelength of 600 nm.

between each trial. The percentage error changes for the same volunteer between different trials. Most plausibly, this is because of the change of the sensor performance due to other measuring artefacts, such as bending that occurs during loading and photobleaching of the sensitive layer, as the conducted measurements are intensity based and ideally require a reference measurement for artefact compensation. Future work will focus on addressing the stability of the sensor's response.

4. Discussion

This study aimed to fabricate and test an OFCS, evaluating its relative performance to commercial sensing systems and its application for monitoring local skin CO_2 during periods of thermal and mechanical load. The study revealed that the OFCS could be manufactured and tested against known standards of CO_2 and corroborated with a commercial sensor. The OFCS achieved a linear response with increasing concentrations of CO_2 within a range of 0–1200 ppm and was characterised by a polynomial over a wider range of CO_2 (up to 46 000 ppm). It is of note that there was a degree of inter-sensor variability in the calibration curves and that the sensors did not return to baseline after removal from the testing environment. The translation of these new OFCSs was demonstrated on a small cohort of healthy volunteers, where increases in local CO_2 were observed during periods of local skin heating and mechanical loads. This demonstrates their potential application to healthcare monitoring, where metabolic markers such as CO_2 can act as a surrogate for a sign of compromised tissue health.

Experiments in a controlled environment demonstrated that there was variability between the responses of the fabricated OFCSs (Fig. 10). This is unsurprising as the sensors were made manually and at different times and therefore will have slightly different TB concentrations and film thicknesses. However, individual calibration enabled the sensors to be used in a skin loading experiment. These variations can be reduced in the future by introducing automation into the manufacturing process.

Throughout the controlled environment and skin loading tests, CO_2 kept increasing for the last 5 min with a 0.5 g load on the skin. The CO_2 concentrations (from the commercial CO_2 sensor) also did not decrease because the stored gas could not escape from the PLA holder as it was a closed gas chamber. Furthermore, the sensor response did not return to
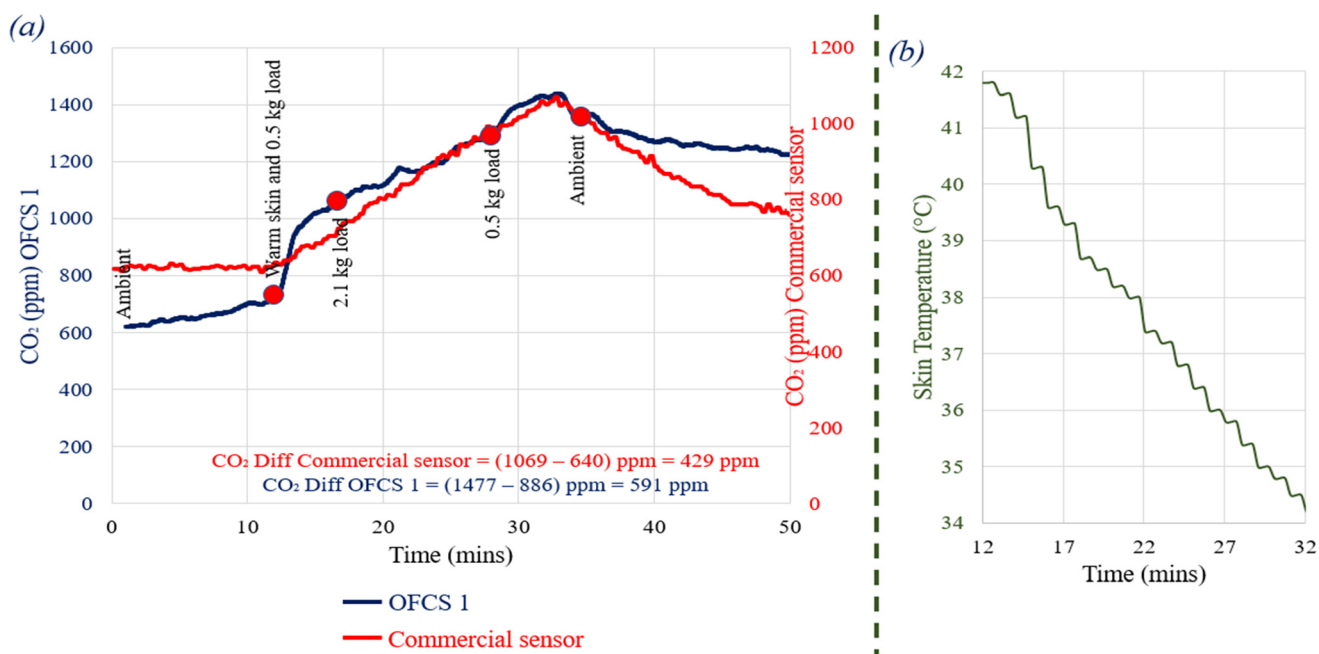

Fig. 11 (a) Response of OFCS 1 and the commercial CO_2 sensor on volunteer 1's forearm. (b) Volunteer 1's skin temperature while a heated disc is on the forearm.

Table 1 Error calculation of CO_2 measurement for 6 volunteers during 3 trials (change in CO_2 between the peak and the baseline)

Volunteer (V) number, OFCS number	Trial (T) number	ΔCO_2 (ppm) commercial sensor	ΔCO_2 (ppm) OFCS	% error
V 1, OFCS 1	T 1	429	591	27.5
	T 2	276	232	18.9
	T 3	266	290	8.3
V 2, OFCS 2	T 1	271	205	32.2
	T 2	165	156	5.8
	T 3	197	136	44.9
V 3, OFCS 3	T 1	261	271	3.7
	T 2	266	265	0.4
	T 3	279	247	12.1
V 4, OFCS 4	T 1	145	168	13.7
	T 2	193	198	2.5
	T 3	180	185	2.7
V 5, OFCS 5	T 1	215	183	17.5
	T 2	267	200	33.5
	T 3	253	182	39.0
V 6, OFCS 6	T 1	199	211	6.0
	T 2	236	243	2.9
	T 3	197	204	3.4

baseline after removal from the environment. The commercial CO_2 sensor returned to baseline during controlled environment testing but did not return to baseline for skin loading, indicating an increase in environmental CO_2 over the duration of the experiment. This partially explains the OFCS not returning to baseline in skin loading, but there are several other possible reasons.

The most likely explanation is that the OFCS response varies due to light exposure to the sensor (photobleaching), which changes the dye properties over time. Another possible reason for not returning to the baseline is the effect of humidity on the ormosil film. The reflection intensity of an OFCS at 600 nm was reduced by 12.4% for the relative humidity (RH) increment between 50% and 70% during a humidity calibration performed inside an environmental chamber (Bench Top, C-TH40-20/1, CVMS Climatic, UK).[22] Also, a drop in reflection intensity of an OFCS at 608 nm was observed due to the RH increment (up to 50%), which indicates the blocking effect of humidity on the permeability of CO_2. The reflection signal of the OFCS changes as CO_2 penetrates through the ormosil film and interacts with the dye–ion pair. CO_2 permeability to the ormosil film determines the OFCS's sensitivity. The ormosil coating has a greater permeability to water molecules due to selective absorption by the silanol group (Si–OH), causing a blocking effect on the pore gas channel, which may restrict CO_2 permeability. Many factors affect the blocking effect such as gas pressure, the film's drying conditions, and pore size.[15]

The film has a slower recovery time compared to the response time because of having more active binding sites before measuring CO_2. CO_2 molecules quickly bind with the absorbing sites from lower to higher CO_2 concentrations. On the other hand, CO_2 molecules diffuse for a long time through the membrane surface (depending on the film thickness and pore size) from higher to lower CO_2 concentrations.[23] These times could be reduced in the future

by decreasing the thickness of the film, although there is a trade-off with reduced absorbance of the film. Although the film was not continuously illuminated, photobleaching also occurs. This could be reduced by using a shutter to expose the film to light for even shorter periods or a modulated light source.

Although the preparation processes of these 6 OFCSs were completely consistent, there were some challenges in manufacturing the OFCSs. For these experiments, a batch of 10 was manufactured while only 6 of these produced spectral absorption features that could be used for CO_2 monitoring. A thin film is created with ormosil on the optical fibre tip using the sol–gel method. Sometimes, severe cracks appear from the dried gel during storage which caused the OFCS absorbance feature to be lost within a few days.

When the number of layers increases, the film thickness rises; consequently, the reflected intensity at a wavelength of around 600 nm declines, as shown in Fig. 5. The absorbance will increase due to film thickness increment, according to eqn (4). It was observed that if the film thickness increases too much (>12 μm), the reflection intensity at a wavelength of 600 nm is below the detection threshold. Another visual observation is that if the film thickness increases too much (>12 μm), the film starts cracking, and the absorbance band at 600 nm is lost. So, the optimum film thickness selection is based on observing the lowest reflection intensity (above 0 counts) while avoiding film cracking.

A thicker film can be achieved while avoiding cracking by raising the dye concentration and reducing the withdrawal speed using the dip coating method.[24,25] Different additives, such as ethylene glycol, can be used in the sol–gel method, preventing the evaporation of the base catalyst (TMAH is volatile) from sol–gel coatings. In addition, the OFCS revealed a moderate diminution in reflection intensity with every single day following fabrication. The OFCS loses its capability for sensing CO_2 within 10–15 days when stored in ambient

air because of the decomposition of the base catalyst (TMAH) inside the film; any chemicals and pollutants in air affect the sensing film and the pH of the sensing film decreases slowly. The OFCS's shelf life (>15 days) and stability in reflectivity may be considerably increased by storing the OFCS in pure N_2.[15]

Our recent publication[26] has demonstrated clearly that a non-ionic surfactant, Triton X-100, improves the stability of the OFCS. Two OFCSs (OFCS 1 and 2) were fabricated without and with Triton X-100 to monitor the stability variation after storage in vacuum-sealed bags in a dark environment for 35 days. The absorbance variation of OFCS 2 (0.813–0.843) was small compared to the absorbance variation of OFCS 1 (0.405–0.177) after 35 days. A PTFE film and Triton X-100 on the OFCS can improve the sensor's long-term stability.[22]

The CO_2 response measured using both sensors was lower than that in previously published research[26] with similar loading. However, in ref. 26, the heating was at a constant temperature of 44.5 °C and the loading was at a bony prominence (sacrum) – both contribute to higher CO_2 levels.

With improvements in the coating as described above, the device has the potential to be used as a monitoring tool. The main advantage of an OFCS is its compact size (diameter = 125 μm). In this research, the sensor was contained in a PLA holder to provide a controlled method of loading and is located behind a PTFE membrane to avoid humidity crosstalk. In practice, the holder could be removed, and the sensors are wrapped in a biocompatible PTFE membrane for comfortable positioning on the skin. This would potentially introduce measurement errors due to motion artefacts and bending; however, an uncoated reference fibre can be used to reduce this effect.[27,28]

5. Conclusion

An OFS has been fabricated and tested on the human skin to measure the skin CO_2 during loading. The reflection intensity of the sensor changes due to variations in the CO_2 concentration emitted from the skin. It was demonstrated that using this platform, a first-in-kind measurement of skin CO_2 with an OFS is possible. The reflection intensity of the 6 OFCSs (OFCS 1–6) changed due to the skin CO_2 concentrations from 145 ppm to 429 ppm within the skin temperature limit of 33.6–41.9 °C. The error range between the 6 OFCSs (OFCS 1–6) and commercial CO_2 sensor was obtained from 6% to 32.2% during the skin CO_2 measurement. There remain some challenges in consistently manufacturing the sensitive film on the tip of the sensor, to achieve reliable and robust results for point-of-care sensing. OFSs are potential tools to measure the skin CO_2 to indicate early events that could lead to the formation of PU.

Data availability

The data supporting this article have been included as part of the ESI.† The datasets generated during and/or analysed

during the current study are not publicly available due to participant privacy and ethical restrictions but are available from the corresponding author on reasonable request.

Conflicts of interest

Declarations of interest: none.

Acknowledgements

References

1 Radiometer, *Solutions for transcutaneous monitoring*, 2014, pp. 2–7, **https://usermanual.wiki/m/0eb48eff7ffc875e1adca939e9129161cab5dcbde075f6df4fbbb82fc6eb4706.pdf** [Accessed: 19 March 2025].

2 A.-M. Kelly and S. Klim, Agreement between arterial and transcutaneous PCO_2 in patients undergoing non-invasive ventilation, *Respir. Med.*, 2011, **105**(2), 226–229, DOI: **10.1016/j.rmed.2010.11.010**.

3 P. von Dadelszen, ABG (Arterial Blood Gas), *The Global Library of Women's Medicine (GLOWM)*, 2001, **https://www.glowm.com/lab-text/item/3#** [Accessed: 19 March 2025].

4 P. Mirtaheri, T. Gjovaag, P. R. Worsley and D. L. Bader, A Review of the Role of the Partial Pressure of Carbon Dioxide in Mechanically Loaded Tissues: The Canary in the Cage Singing in Tune with the Pressure Ulcer Mantra, *Ann. Biomed. Eng.*, 2015, **43**(2), 336–347, DOI: **10.1007/s10439-014-1233-z**.

5 Prevention and treatment of pressure ulcers/injuries: Quick reference guide, *European Pressure Ulcer Advisory Panel, National Pressure Injury Advisory Panel and Pan Pacific Pressure Injury Alliance*, ed. E. Haesler, 3rd edn, 2019, p. 43, ISBN: 978-0-6480097-9-5.

6 A. Gefen, Reswick and Rogers pressure-time curve for pressure ulcer risk. Part 1, *Nurs. Stand.*, 2009, **23**(45), 64–68, DOI: **10.7748/ns2009.07.23.45.64.c7115**.

7 S. Coleman, J. Nixon, J. Keen, L. Wilson, E. McGinnis, C. Dealey, N. Stubbs, A. Farrin, D. Dowding, J. M. G. A. Schols, J. Cuddigan, D. Berlowitz, E. Jude, P. Vowden, L. Schoonhoven, D. L. Bader, A. Gefen, C. W. J. Oomens and E. A. Nelson, A new pressure ulcer conceptual framework, *J. Adv. Nurs.*, 2014, **70**(10), 2222–2234, DOI: **10.1111/jan.12405**.

8 J. L. Zeller, C. Lynm and R. M. Glass, Pressure Ulcers, *JAMA, J. Am. Med. Assoc.*, 2006, **296**(8), 1020, DOI: **10.1001/jama.296.8.1020**.

9 Y. Brazier, *Bed sores or pressure ulcers: What you need to know*, Medical News Today, 2020, **https://www.medicalnewstoday.com/articles/173972** [Accessed: 19 March 2025].

10 W. van Weteringen, T. G. Goos, T. van Essen, C. Ellenberger, J. Hayoz, R. C. J. de Jonge, I. K. M. Reiss and P. M. Schumacher, Novel transcutaneous sensor combining optical t_CPO_2 and electrochemical t_CPCO_2 monitoring with reflectance pulse oximetry, *Med. Biol. Eng. Comput.*, 2020, **58**(2), 239–247, DOI: **10.1007/s11517-019-02067-x**.

11 Radiometer, *The tcpCO₂ Handbook*, 2011, pp. 7–31, **https://mss.co.th/media/trancutaneous/TC100_Understanding_transcutaneous%20pO2_and_pCO2/tcpco2handbook.pdf** [Accessed: 19 March 2025].

12 Radiometer, *Safety Data Sheet of Chemicals for Radiometer Equipment*, 2013, pp. 1–10, **https://punchout.medline.com/media/catalog/Docs/MSDS/MSD_SDSD80360.pdf** [Accessed: 19 March 2025].

13 Radiometer, *TCM4 and TCM40 Specifications*, 2008, pp. 2–3, **https://www.pulmodata.si/veleprodaja/pdf/TCM4.pdf** [Accessed: 19 March 2025].

14 N. Sabri, S. A. Aljunid, M. S. Salim and S. Fouad, Fibre Optic Sensors: Short Review and Applications, *Recent Trends in Physics of Material Science and Technology*, Springer Series in MaterialsScience, 2015, vol. 204, pp. 299–311, DOI: **10.1007/978-981-287-128-2_19**.

15 L. L. Liu, F. H. Hao, S. P. Morgan, R. Correia, A. Norris and S. Korposh, A reflection-mode fibre-optic sensor for breath carbon dioxide measurement in healthcare, *Sens. Biosensing Res.*, 2019, **22**, 1–8, DOI: **10.1016/j.sbsr.2018.100254**.

16 S.-K. Lee and I. Okura, Porphyrin-doped sol-gel glass as a probe for oxygen sensing, *Anal. Chim. Acta*, 1997, **342**(2–3), 181–188, DOI: **10.1016/S0003-2670(96)00562-4**.

17 S. Ahangarani, N. Lari and A. Shanaghi, Influence of TEOS concentration and Triton additive on the nanostructure silica sol-gel anti-reflective coatings, *Int. J. Mater. Prod. Technol.*, 2017, **55**(4), 319–330, DOI: **10.1504/IJMPT.2017.087027**.

18 K. Ertekin, C. Karapire, S. Alp, B. Yenigul and S. Icli, Photophysical and photochemical characteristics of an azlactone dye in sol-gel matrix; a new fluorescent pH indicator, *Dyes Pigm.*, 2003, **56**(2), 125–133, DOI: **10.1016/S0143-7208(02)00125-0**.

19 P. Worsley and D. Voegeli, Back to basics: biophysical methods in tissue viability research, *J. Wound Care*, 2013, **22**(8), 434–439, DOI: **10.12968/jowc.2013.22.8.434**.

20 L. L. Liu, S. P. Morgan, R. Correia and S. Korposh, A single-film fiber optical sensor for simultaneous measurement of carbon dioxide and relative humidity, *Opt. Laser Technol.*, 2022, **147**(107696), 1–9, DOI: **10.1016/j.optlastec.2021.107696**.

21 P. Ewart, *Optics: the science of light, Lecture notes of 2nd year Physics FHS A2*, University of Oxford, 2014, p. 36, **https://users.physics.ox.ac.uk/~ewart/Optics%202011%20%20Part%201%20slides.pdf** [Accessed: 19 March 2025].

22 N. Afroze, S. Korposh, R. Correia, B. R. Hayes-Gill, S. Lee and S. P. Morgan, Improving the Stability in Intensity and Absorbance of an Optical Fiber CO_2 Sensor, *4th International Conference on Robotics, Electrical and Signal Processing Techniques (ICREST)*, Dhaka, Bangladesh, 2025, pp. 96–99, DOI: **10.1109/ICREST63960.2025.10914412**.

23 W. Ma, R. Wang, Q. Rong, Z. Shao, W. Zhang, T. Guo, J. Wang and X. Qiao, CO_2 Gas Sensing Using Optical Fibre Fabry-Perot Interferometer Based on Polyethyleneimine/Poly(Vinyl Alcohol) Coating, *IEEE Photonics J.*, 2017, **9**(3), 1–8, DOI: **10.1109/JPHOT.2017.2700053**.

24 C. J. Brinker, *Dip Coating, Chemical Solution Deposition of Functional Oxide Thin Films*, Springer, 2013, ch. 10, pp. 237–238, ISBN: 978-3-211-99310-1.

25 K. Wysokiński, M. Napierała, T. Stańczyk, S. Lipiński and T. Nasiłowski, Study on the sensing Coating of the Optical Fibre CO_2 Sensor, *Sensors*, 2015, **15**(12), 31888–31903, DOI: **10.3390/s151229890**.

26 N. Afroze, S. Korposh, R. Correia, B. R. Hayes-Gill, S. Lee and S. P. Morgan, Improving the Stability in Intensity and Absorbance of an Optical Fiber CO2 Sensor, *4th International Conference on Robotics, Electrical and Signal Processing Techniques (ICREST)*, Dhaka, Bangladesh, 2025, pp. 96–99, DOI: **10.1109/ICREST63960.2025.10914412**.

27 S. L. Knight, R. P. Taylor, A. A. Polliack and D. L. Bader, Establishing predictive indicators for the status of loaded tissues, *J. Appl. Physiol.*, 2001, **90**(6), 2231–2237, DOI: **10.1152/jappl.2001.90.6.2231**.

28 C. He, S. Korposh, F. U. Hernandez, L. Liu, R. Correia, B. R. Hayes-Gill and S. P. Morgan, Real-Time Humidity Measurement during Sports Activity using Optical Fibre Sensing, *Sensors*, 2020, **20**(7), 1–12, DOI: **10.3390/s20071904**.